ARTICLE

Metal-dependent assembly of a protein nano-cage

Ajitha S. Cristie-David[1] | E. Neil G. Marsh[1,2]

[1]Department of Chemistry, University of Michigan, Ann Arbor, Michigan

[2]Department of Biological Chemistry, University of Michigan, Ann Arbor, Michigan

Correspondence
E. Neil G. Marsh, Department of Chemistry, University of Michigan, Ann Arbor, MI 48109.
Email: nmarsh@umich.edu

Funding information
Army Research Office, Grant/Award Number: W911NF-16-1-0147

Abstract

Short, alpha-helical coiled coils provide a simple, modular method to direct the assembly of proteins into higher order structures. We previously demonstrated that by genetically fusing de novo–designed coiled coils of the appropriate oligomerization state to a natural trimeric protein, we could direct the assembly of this protein into various geometrical cages. Here, we have extended this approach by appending a coiled coil designed to trimerize in response to binding divalent transition metal ions and thereby achieve metal ion-dependent assembly of a tetrahedral protein cage. Ni^{2+}, Co^{2+}, Cu^{2+}, and Zn^{2+} ions were evaluated, with Ni^{2+} proving the most effective at mediating protein assembly. Characterization of the assembled protein indicated that the metal ion–protein complex formed discrete globular structures of the diameter expected for a complex containing 12 copies of the protein monomer. Protein assembly could be reversed by removing metal ions with ethylenediaminetetraacetic acid or under mildly acidic conditions.

KEYWORDS
coiled coils, metalloproteins, protein design, protein nano-cages

1 | INTRODUCTION

Protein-based nanoparticles, both natural and designed, have gained increasing attention as promising materials for a wide variety of applications in nanotechnology, nanomedicine, and materials science.[1–15] The growing interest in protein-based materials has stimulated interest in designing new protein assemblies of various architectures that incorporate structural and functional properties that extend beyond those found in *Nature*. The assembly of protein building blocks (PBB) into large-scale cage-like structures has been accomplished through different approaches; these include the design of new protein–protein interfaces,[16–18] the fusion of oligomeric protein domains,[19,20] and by using de novo–designed oligomeric coiled coils to connect together larger, natural proteins.[21–24]

Our laboratory has focused on this latter approach.[21–26] Using parallel coiled coils that form well-specified trimeric, tetrameric, and pentameric helical bundles, we have assembled a natural trimeric protein into, respectively, tetrahedral,[22] octahedral,[21] and icosahedral cage-like structures.[23] These

protein cages were constructed by genetically fusing the coiled coil domain to the C-terminus of the natural protein through an oligo-glycine linker sequence. Efficient assembly of the protein cages was achieved by optimizing the oligo-glycine linker length. This approach provides a simple, symmetry-based route for assembling protein cages that does not require extensive computational modeling and protein engineering.

A further challenge in the design of self-assembling proteins is to control the assembly process. Natural multimeric proteins such as actin,[27] the vertebrate nuclear pore complex,[28] and some viral capsids[29] undergo environmentally responsive assembly and disassembly. Inspired by *Nature*, various strategies have been developed to control the assembly of extended protein-based nanomaterials that form filaments,[30,31] 2D lattices,[32,33] and 3D crystals.[34–36] Assembly has been controlled by, for example, the judicious use of protein–protein disulfide linkages,[33,37] the use of bifunctional small molecules[38] to connect together protein subunits and the design of "split" metal ion-binding sites[30,31,33,36,39,40] that span two protein subunits. Natural protein cages such as ferritin have been

reengineered to undergo environmentally responsive assembly and disassembly; for example, a Cu(II)-responsive ferritin cage was designed by introducing His residues at the inter-subunit interface of ferritin,[41] whereas a pH-responsive ferritin cage was engineered by introducing a pH-responsive amphipathic helix into the inter-subunit interface.[42] Most recently, a protein cage designed to assemble in response to binding gold ions has been described.[43]

In this work, we have extended our coiled coil-based strategy for assembling proteins to design a cage that assembles and disassembles in response to binding divalent transition metal ions. We utilized a metal-dependent coiled coil design (IZ-3adH)[44] that was previously shown to assemble into a homo-trimeric parallel coiled coil in the presence of divalent transition metal ions (Figure 1) and genetically fused it to a trimeric protein to facilitate the metal-dependent assembly of this protein into a tetrahedral structure (Figure 2). In the presence of divalent metal ions, this construct assembled into discrete-high M_w particles consistent with the formation of a tetrahedral protein cage. Protein assembly could be reversed either by the addition of metal chelators or by decreasing the pH.

2 | RESULTS

2.1 | Design of a metal-dependent protein cage

To facilitate comparison with our previous studies, we employed the same trimeric esterase (TriEst; PDB ID: 1ZOI) as the PBB that we previously used to assemble tetrahedral,[22] octahedral,[21] and icosahedral[23] protein cages. To make the assembly of TriEst into a metal ion dependent tetrahedral cage, we

selected a de novo–designed 4-heptad coiled coil[44] that was previously designed to oligomerize into a parallel trimeric 3-helix bundle in the presence of divalent transition metal ions. A metal-binding site was introduced into the coiled coil by incorporating His residues at *a* and *d* positions in the third heptad repeat to provide a potentially six-coordinate metal-binding site (Figure 1). The peptide was shown to assemble into a trimeric coiled coil in the presence of divalent transition metals such as Ni^{2+}, Co^{2+}, Cu^{2+}, and Zn^{2+} and returned to an unstructured monomeric form upon removal of metals or when the pH was lowered beyond ∼5.5, when the histidine residues are presumably protonated.

We genetically fused this metal-binding coiled coil to the C-terminus of TriEst through a flexible 8-residue linker sequence (GTGGGGGG) that had been optimized in the original tetrahedral protein cage design[22] (Figure 2a). Although previous designs used a His-tag to facilitate protein purification, in this case, we were concerned that a nickel-binding tag could interfere with metal binding. Therefore, a maltose-binding protein (MBP; PDB ID: 1ANF) domain was appended to the N-terminus of TriEst through a 17-residue spacer to facilitate purification. This fusion construct was named as Tet8-M, to signify that it was designed to form a **Tet**rahedral cage with an **8**-residue spacer sequence separating the PBB from the **M**etal-binding coiled coil (Figure 2a,b, Table S1).

Tet8-M was overexpressed in *Escherichia coli* and purified to homogeneity, as judged by sodium dodecyl sulfate-polyacrylamide gel electrophoresis (SDS-PAGE), by MBP affinity column chromatography followed by size exclusion chromatography, as described in Section 4. The addition of the MBP domain also resulted in a significantly higher yield
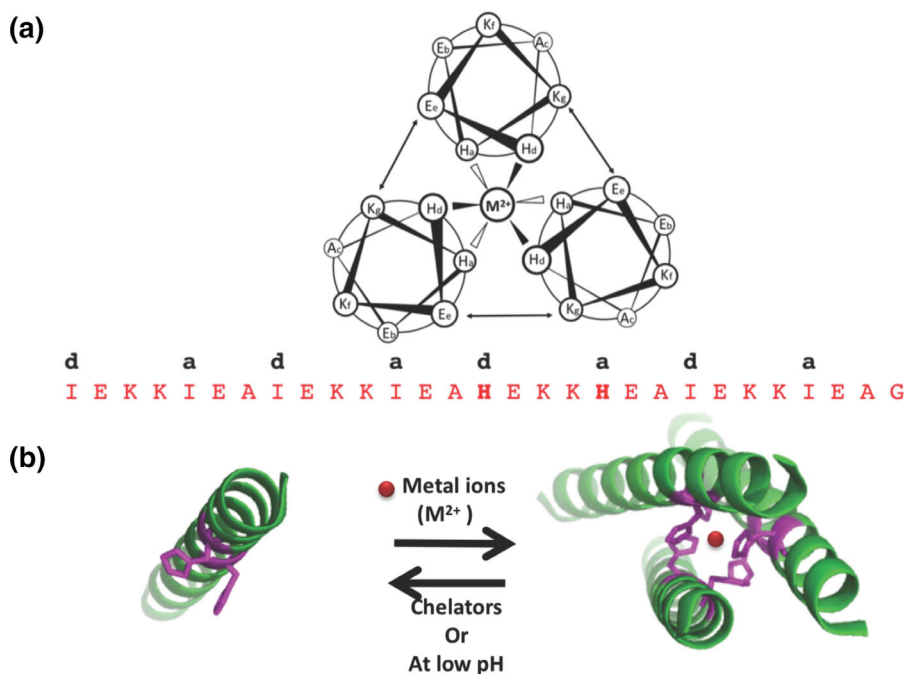
(a)

(b)

FIGURE 1   Metal dependent IZ-3adH coiled coil motif. (a) N-terminus view of helical wheel representation of the third heptad (*top*) and the peptide sequence (*bottom*) of IZ-3ad. His residues at the third "a" and "d" positions form a metal binding site with potential six-coordinate geometry. (b) A cartoon illustrating the metal-dependent trimerization of IZ-3adH mediated through metal ligation by histidine residues
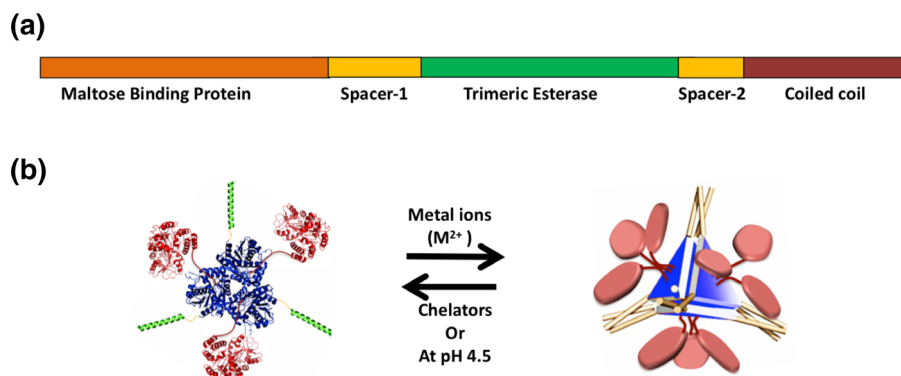
(a)

(b)

FIGURE 2 Outline of the strategy used to construct the metal-dependent protein cage. (a) Domain structure of the Tet8-M fusion protein. (b) Cartoon illustrating the metal-induced assembly of Tet8-M
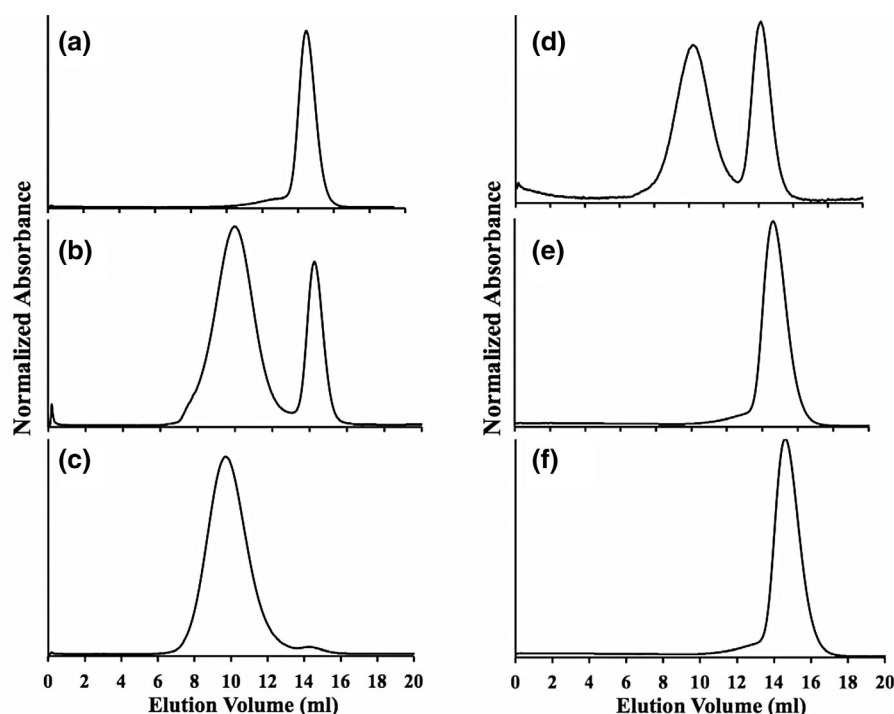

FIGURE 3 Size exclusion chromatography of Tet8-M under various conditions. (a) Chromatography of Tet8-M trimers after purification. (b) Chromatography of Tet8-M, 20 μM, after equilibration with 80 μM Ni^{2+}. (c) Re-chromatography of the Ni^{2+}-Tet8-M complex with 20 μM Ni^{2+} added to the buffer. (d) Re-chromatography of the Ni^{2+}-Tet8-M complex in the absence of Ni^{2+} in the buffer. (e) Re-chromatography of the Ni^{2+}-Tet8-M complex in the presence of 2 mM EDTA. (f) Re-chromatography of the Ni^{2+}-Tet8-M complex at pH 4.5 in buffer containing Ni^{2+}

of purified protein, ∼400 mg/L of culture, compared to previous designs that employed a His-tag for purification. The purified protein was dialyzed overnight at 4°C in buffer containing 2 mM ethylenediaminetetraacetic acid (EDTA) to remove any bound metal ions. Size exclusion chromatography (SEC) of Tet8-M on a superose 6 10/300 column showed Tet8-M to elute as a single symmetrical peak at 14.5 mL, which is consistent with the expected $M_r = 227.4$ kDa for the trimeric form of the protein (Figure 3a).

Our original intention was to remove the MBP domain from Tet8-M by incorporating a tobacco etch virus (TEV) protease cleavage site into the spacer sequence between the MBP and TriEst domains. However, this strategy proved unsuccessful because, for reasons that are unclear, digestion of Tet8-M with TEV protease proceeded extremely slowly, requiring ∼2 weeks to approach completion. The TEV-cleaved protein did not form well-defined complexes in response to the

addition of metal ions, possibly due to degradation during the prolonged cleavage reactions. Therefore, the full-length Tet8-M protein was used in all the experiments. The addition of the large MBP domain, which is separated from the trimeric esterase domain by a 13-residue spacer, did not seem to interfere with the assembly process.

2.2 | Equilibrating Tet8-M with metal ions

The de novo–designed metal-binding coiled coil (IZ-3adH) was originally reported to have low micromolar affinities for several divalent metal ions with relative affinities in the order $Ni^{2+} > Cu^{2+} > Co^{2+} \approx Zn^{2+}$.[44] We therefore evaluated the potential of the Tet8-M construct to assemble into protein cages in the presence of these metal ions. Because Ni^{2+} was reported to have the highest affinity for the peptide ($K_d = 5.0 \pm 0.3$ μM), we first studied the binding of Ni^{2+} by

Tet8-M. A solution of 20 μM Tet8-M was equilibrated with concentrations of NiCl$_2$ varying from 5 to 200 μM at 4°C with gentle stirring overnight. The samples were then analyzed by SEC on a superose 6 10/300 column equilibrated with Tris-HCl buffer, pH 8.0, containing the same NiCl$_2$ concentrations. Two peaks were observed for all the samples, at 10.5 and 14.5 mL indicating that some of the protein was assembling into higher molecular weight species (Figure 3B, Appendix S1). Ni^{2+} concentrations between 20 and 200 μM resulted in the largest fraction of Tet8-M being converted to high molecular weight species. Analysis of the peak areas indicated that approximately 65–75% of the protein was assembled into high molecular weight species at these Ni^{2+} concentrations (Figure S1b). The behavior of Tet8-M was studied at higher Ni^{2+} concentrations of 1 and 2 mM; however, this resulted in a decrease in the fraction (~30–40%) of protein assembling into high molecular weight species. Equilibrating Tet8-M with Ni^{2+} ions at room temperature or for longer periods of time (up to 2 weeks) did not make any significant difference to the size distribution of Tet8-M species.

We also examined the effectiveness of Co^{2+}, Cu^{2+}, and Zn^{2+} ions to mediate the assembly of Tet8-M. Of note, 20 μM samples of Tet8-M were equilibrated with 20, 80, and 200 μM concentrations of each metal ion and evaluated by SEC. Co^{2+} ions were found to be similarly as effective as Ni^{2+} in mediating the formation of high molecular weight species at all the metal ion concentrations examined (Figure S2a). However, whereas lower concentrations of Cu^{2+} mediated formation of a protein complex of the expected size, incubation of Tet8-M with 200 μM Cu^{2+} resulted in the protein eluting at a volume of 12 mL, indicating a complex smaller than expected, in addition to unassembled protein that eluted at 14.5 mL. Four-coordinate complexes are also common for Cu^{2+}, so the peak at elution volume 12 mL might result from Tet8-M forming dimers with Cu^{2+} ions (Figure S2b). In support of this possibility, Suzuki et al. previously observed dimer formation with IZ-3adH peptides at higher Cu^{2+} concentrations, whereas at low Cu^{2+} concentrations IZ-3adH formed trimers.[44] Zn^{2+} ions proved only to be effective at assembling Tet8-M at the lowest concentrations used (20 μM). At higher concentrations, only a single peak at elution volume 14.5 mL corresponding to unassembled material was observed (Figure S2c). The reason for this is unclear, but we note that the pseudo-octahedral metal binding site provided by the trimeric peptide is not optimal for binding zinc because the preferred geometry is for zinc in proteins is tetrahedral.

2.3 | Characterization of Ni^{2+}-mediated assembly of Tet8-M

As Ni^{2+} ions appeared to be the most effective at causing the oligomerization of Tet8-M, subsequent characterization of the design focused on this metal. The high-molecular-weight oligomers formed by the Ni^{2+}-Tet8-M complex were purified by equilibrating the protein overnight with 200 μM NiCl$_2$, and the oligomers separated from unassembled protein by SEC in the presence of NiCl$_2$. When re-chromatographed in buffer containing NiCl$_2$, the assembled protein eluted at the same elution volume in a symmetrical peak (Figure 3c). This suggested the assembled protein was fairly homogeneous and that, once formed, the assemblies were kinetically stable and did not re-equilibrate to form a mixture of assembled and unassembled species. In contrast, when the assembled species were re-chromatographed in buffer lacking divalent metal ions, the protein eluted as a mixture of assembled and unassembled forms (Figure 3d). This is consistent with the loss of Ni^{2+} ions from the complex during chromatography. Complete disassembly of the complex could be achieved by subjecting the samples to SEC in Tris-HCl buffer containing 2 mM EDTA. This resulted in Tet8-M eluting as a single peak at elution volume ~14.5 mL, indicating complete dissociation of the complex into the original trimeric form (Figure 3e). Similar results were observed when the assembled protein complexes were re-chromatographed with buffer adjusted to pH 4.5, which again resulted in the protein eluting ~14.5 mL (Figure 3f).

Disassembly of the protein cages appeared to be reversible. Removing the EDTA by dialysis, followed by re-equilibrating the protein with Ni^{2+}, resulted in most of the protein reassembling (as judged by SEC; Figure S3a) to give a distribution of assembled and unassembled species that was similar to the initially constituted material. Readjusting the pH of the acid-dissociated protein from pH 4.5 to pH 8.0 similarly resulted in the protein reassembling to give a distribution of assembled and unassembled species (Figure S3b). However, for the acid-dissociated cages, SEC of the reassembled material also indicated a small amount of aggregated protein, evident in the void volume, which might have resulted from denaturation of some of the TriEst domain at low pH (Figure S3b). In support of this, previous studies have demonstrated that TriEst has reduced activity and stability at acidic pH and completely loses activity at pH 3.[45,46]

2.4 | Characterization of metal dependent assembly of Tet8-M

2.4.1 | Dynamic light scattering

Dynamic light scattering (DLS) is widely used to measure the hydrodynamic radius of particles and to assess the homogeneity of samples; therefore, we examined the effect of Ni^{2+} ions on the particle size of Tet8-M. Scattering spectra were recorded for 20 μM solutions of Tet8-M at pH 8.0 in Tris–HCl buffer in the absence of divalent metal ions and in the presence of 100 μM NiCl$_2$. In the absence of metal ions,

the number-averaged hydrodynamic diameter was 11.9 ± 1.0 nm, which is consistent with the modeled diameter of ~12 nm for the trimeric form of the protein (Figure 4). In the presence of Ni^{2+} ions, the number-averaged hydrodynamic diameter of Tet8-M increased to 23.8 ± 0.9 nm, which is in reasonable agreement with the calculated diameter of ~20 nm for a tetrahedral protein cage assembly (Figure 4).

DLS spectra of Tet8-M were recorded after the Ni^{2+} ions were removed from the assembled protein by chelation with EDTA or the pH reduced to 4.5 to dissociate the coiled coils (Figure 4). The number-averaged hydrodynamic diameter for the EDTA-treated sample was 12.6 ± 0.4 nm and that for the low-pH sample, which showed some heterogeneity,
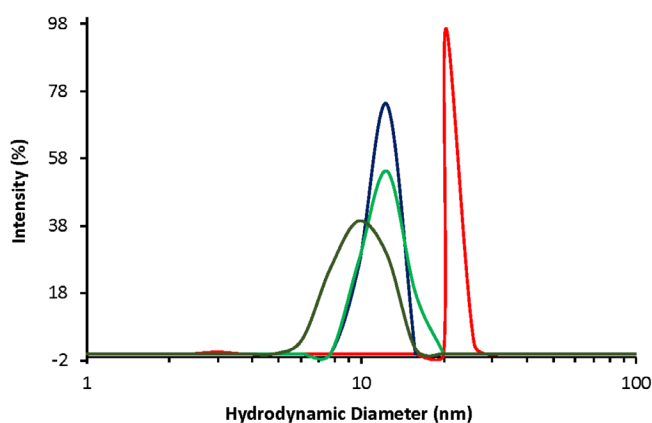
was 7.9 ± 1.0 nm. These results are consistent with the Tet8-M returning to a trimeric state, as indicated by the SEC experiments described above.

2.4.2 | Native-PAGE

The assemblies formed by Tet8-M were further studied by native-PAGE, as this technique provides a sensitive method to assess the homogeneity of protein assemblies. The protein subunits of the Ni-Tet8-M complex were cross-linked using the lysine-selective cross-linking reagent bis(sulfosuccinimidyl) suberate (BS3) prior to electrophoresis (Figure 5A and Figure S4a). This was necessary to prevent dissociation of the assembled material because the electrophoresis conditions stripped the Ni^{2+} ions from the protein. Samples were analyzed on a 3–12% gradient polyacrylamide gel (Figure 5b and Figure S4b). Both the cross-linked Ni^{2+}-Tet8-M complex and the non-cross-linked sample migrated as somewhat diffuse bands, but otherwise appeared fairly homogenous. The cross-linked Tet8-M sample migrated as a much larger species than the untreated Tet8-M sample, indicating Ni-mediated assembly of the protein (Figure 5b and Figure S4b). Control experiments confirmed that treating Tet8-M with BS3 in the absence of Ni^{2+} ions did not cause crosslinking into high molecular weight material (Figure 5b and Figure S4b).

2.4.3 | Electron microscopy

The particles formed by Tet8-M were visualized by negative-stain transmission electron microscopy. The trimeric form of the protein (fractions from elution volume 14.5 mL) appeared as small, unassembled species by electron microscopy (EM; Figure 6a). In preliminary experiments, we found that the Ni^{2+}-Tet8-M complexes partly dissociated on the EM grids

FIGURE 4 Hydrodynamic diameter of complexes formed by Tet8-M analyzed by DLS. Dark blue trace: Tet8-M in the absence of metal ions; red trace: Tet8-M in the presence of Ni^{2+} ions; lime green trace: Ni^{2+}-Tet8-M complexes after treatment with EDTA; dark green trace: Ni^{2+}-Tet8-M complexes after reducing the pH to 4.5. DLS, dynamic light scattering; EDTA, ethylenediaminetetraacetic acid
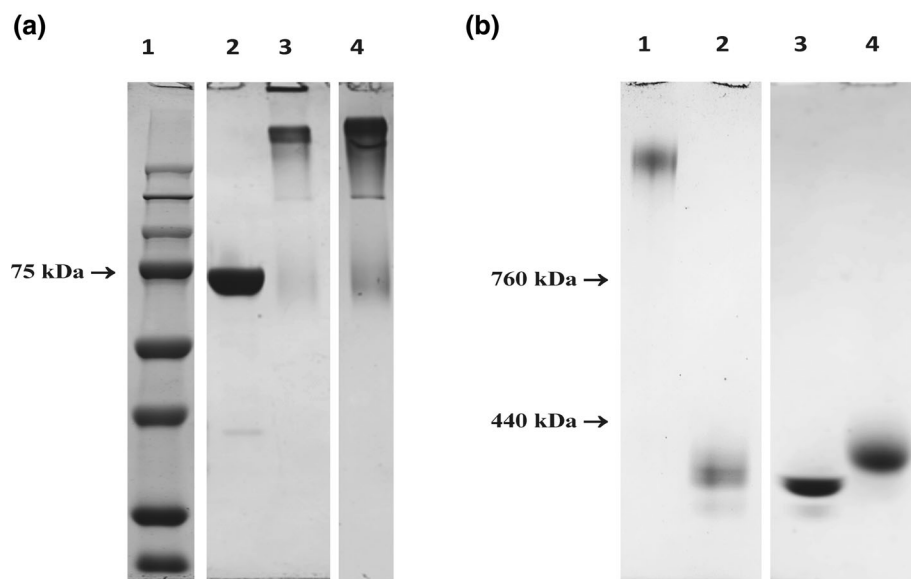
FIGURE 5 Electrophoretic analysis of Tet8-M. (a) SDS-PAGE of Tet8-M: lane 1—molecular weight markers; lane 2—Tet8-M, non-cross-linked and in the absence of Ni^{2+}; lane 3—Tet8-M cross-linked in the presence of Ni^{2+}; lane 4—Tet8-M cross-linked in the absence of Ni^{2+}. (b) Native PAGE of Tet8-M: lane 1—Tet8-M assembled in the presence of Ni^{2+} and cross-linked; lane 2—Tet8-M assembled in the presence of Ni^{2+} without cross-linking; lane 3—Tet8-M, non-cross-linked and in the absence of Ni^{2+}; lane 4—Tet8-M cross-linked in the absence of Ni^{2+}. Positions of native PAGE molecular weight markers are indicated

FIGURE 6 Negative-stain transmission electron microscopy (TEM) of Tet8-M complexes. (a) Purified, unassembled Tet8-M. (b) Ni^{2+}-Tet8-M complexes imaged without cross-linking show a background of dissembled trimers. (c, d) SEC purified and cross-linked Ni^{2+}-Tet8-M complexes images at 2 magnifications. (e) Size distribution analysis of cross-linked Ni^{2+}-Tet8-M particles imaged by negative stain TEM
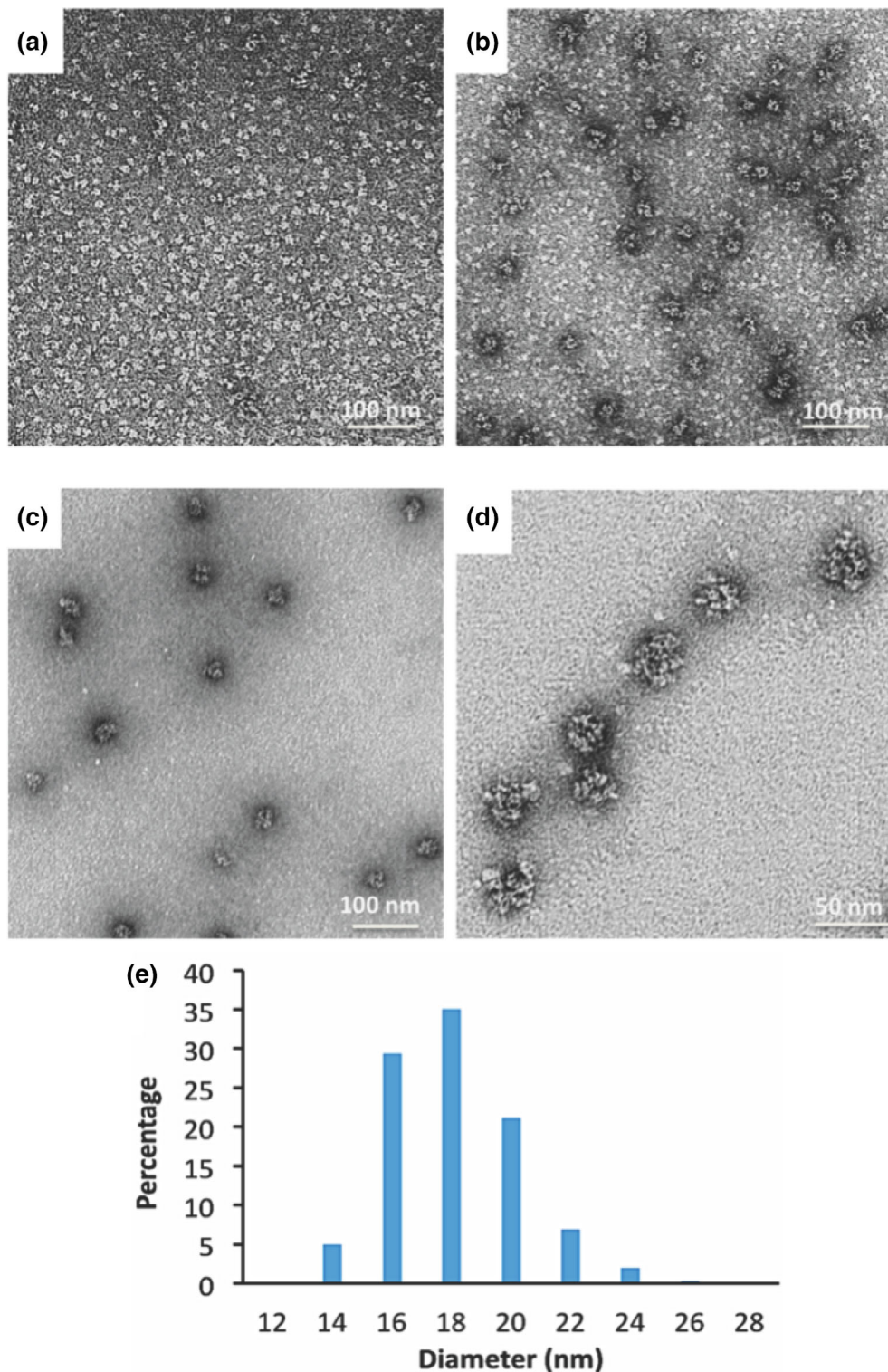
during sample preparation. This was not observed for our previous cage designs and might be due to interactions between the coiled coils domains and Cu ions on the surface of the TEM grid (Figure S5). This problem was overcome by covalently crosslinking the assembled protein with BS3 reagent, as described above (Figure 5a and Figure S4a). The cross-linked material appeared as discrete, homogenous particles (Figure 6c,d). However, for most of the particles, neither details of the symmetry nor the shape of the particles could be discerned in the TEM images, possibly because the peripheral MBP domain linked to TriEst masked the core structure. The diameter distribution of TEM images analyzed using Image J software gave an average diameter of ~18 nm for the particles (Figure 6e).

2.4.4 | Catalytic activity

The esterase activities of the trimeric Tet8-M construct and the high-molecular-weight species assembled from Tet8-M in the presence of Ni^{2+} were compared with the unmodified esterase, TriEst, from which Tet8-M is derived. With *2,4*-dinitrophenyl acetate (*2,4*-DNPA) as a substrate, the turnover number for unmodified TriEst was 14.2 ± 2.3 min^{-1}, whereas the turnover number for trimeric Tet8-M was 22.3 ± 1.9 min^{-1} and turnover number for the Ni- Tet8-M complex was 15.5 ± 1.7 min^{-1}. These results confirmed that neither the assembly process nor fusion of the coiled coil with MBP domain significantly alters the functional properties of TriEst.

3 | DISCUSSION

There has been extensive interest in creating metal-dependent protein assemblies that may have uses as sensors or responsive biomaterials.[33,34,36,39,40,43] The experiments we describe here demonstrate the potential of using metal-binding coiled coils to mediate protein assembly, a concept that could be extended to other environmentally responsive coiled coil designs.

Characterization of the complex formed by Tet8-M with Ni^{2+} ions using SEC, DLS, TEM, and native-PAGE were all consistent with the trimeric PBB assembling into the intended tetrameric structure. The hydrodynamic radius determined by DLS and the diameter determined by analysis of negative stain TEM images were in a good agreement with the diameter predicted from simple molecular modeling ($\sim$20 nm). For our previously designed protein cages, it was possible to obtain structural information on the geometry of the cage from cryo-EM; however, in this case, it was not possible to verify that Tet8-M adopts at tetrahedral structure using this technique. The MBP domain, which proved necessary to obtain sufficient yields of soluble protein, probably masks the core cage structure so that the symmetry of the assembled structures was not apparent in most of the particles imaged by negative stain TEM.

Although conceptually simple and easily accomplished, our approach also illustrates some of the problems inherent in constructing ligand-responsive protein assemblies. The Tet8-M construct assembled into higher order species with each of the divalent metal ions examined; however, despite varying the metal ion concentrations and other conditions, it was not possible to achieve complete assembly of the trimeric building block. Even under the most favorable conditions, only 65–75% of the protein assembled and, interestingly, higher metal ion concentrations inhibited assembly. Once assembled, the metal–protein complex appeared stable and could be readily purified from the unassembled material by SEC.

Either treating the assembled protein with chelating agents or lowering the pH of the buffer led to disassembly of the cages. The protein could then be reassembled by removing the chelating agent and incubating with metal ions or raising the pH, confirming that the assembly process is fully reversible. However, reassembly resulted in a similar ratio of assembled cages to unassembled protein being formed (as judged by SEC) as seen initially. One explanation is that metal ions may form coordination complexes within the same trimeric PBB so that the coiled coil domains are not available to interact with other subunits and so become kinetically trapped in unproductive conformations. This observation points to the importance of optimizing the strength of the metal–protein interaction in addition to the coiled coil interaction to achieve efficient assembly. We note that the pseudo-octahedral metal binding site afforded by positioning histidine residues at "a" and "d" positions of the coiled coil heptad (Figure 1) provides a fairly crude mimic of the metal binding sites found in natural metalloproteins. Indeed, we are not aware of any natural example of a "6-His" metal binding site. The metal binding sites of natural proteins nearly always comprise more than one type of side-chain and are fine-tuned by second sphere interactions with the primary coordination sphere.

In conclusion, we successfully constructed a metal-dependent protein cage by utilizing a symmetry-based design strategy together with coiled coil sequences that oligomerize in response to binding divalent transition metal ions. However, although reversible, the assembly process was not highly efficient and depended critically on the metal ion concentrations used to mediate oligomerization, likely because some of the Tet8-M protein became trapped in nonproductive metal–protein complexes. These observations illustrate the need to optimize the strength of both the coiled coil interaction and the metal-binding interaction to achieve efficient assembly.

4 | MATERIALS AND METHODS

4.1 | Construction of gene encoding Tet8-M

A synthetic gene encoding the metal-binding coiled coil sequence together with a $5'$-sequence encoding an 8-Gly spacer sequence was commercially synthesized. This DNA sequence was genetically fused to the $3'$-end of the gene encoding TriEst housed in the expression vector pET-28B using standard protocols. The MBP domain encoded by the plasmid pMAL-c5X was subsequently fused to the N-terminus of TriEst through a 17-residue spacer sequence (GGGGGGGGGGGENLYFQGG) by standard protocols to give the final Tet8-M fusion protein. The complete sequence of the Tet8-M design is given in Table S1.

4.2 | Protein expression and purification

Protein was expressed using standard methods as previously described.[21] Briefly, the protein was expressed in *E. coli* BL21(DE3) cells grown in 2xYT medium with 100 mg/L ampicillin at 37°C. At an OD_{600} of 0.8, the temperature was reduced to 18°C, and at an OD_{600} of 1.0, protein expression was induced by addition of IPTG to 0.1 mM final concentration. Cells were grown for a further 18 hr, harvested by centrifugation and stored at −80°C.

Protein was purified using maltose affinity column chromatography as previously described[21,24] and summarized here. All purification steps were performed on ice or at 4°C. Approximately 4 g of cell pellet were thawed on ice for ~20 min, resuspended in buffer containing 50 mM HEPES, 100 mM ammonium acetate, 5% glycerol, 1 FAST protease inhibitor tablet (Sigma), and ~50 mg of chicken egg lysozyme (Sigma), and gently agitated for ~15–20 min. Cells were lysed by sonication (10 s "ON", 30 s "OFF" for 10 min), and the lysate was clarified by centrifugation at $40,000g$ for 20 min. The supernatant was loaded on to a 5 mL MBP-trap column (GE Healthcare) at a flow rate of 0.5 mL/min. The column was washed with ~80 mL of the same buffer at a flow rate of 1 mL/min and then the protein eluted at a flow rate of 0.5 mL/min with buffer containing 10 mM maltose, 50 mM HEPES, 100 mM ammonium acetate, and 5% glycerol. Fractions containing the desired protein (approximately 10–15 mL) were combined and treated with 2 μL of Benzonase. The resulting solution was dialyzed against buffer containing 20 mM HEPES, 100 mM ammonium acetate, 2 mM EDTA, and 10% glycerol approximately for 2 days at 4°C.

SEC was used as an additional purification step and to assess the molecular weights of the complexes formed by Tet8-M. SEC was performed on a superose-6 10/300 column equilibrated with Tris HCl SEC buffer (10 mM Tris HCl, 100 mM NaCl, pH 8.0) at 4°C. Of note, 400 μL injections of samples at concentrations of 2–3 mg/mL were chromatographed at a 0.3 mL/min flow rate. Trimeric Tet8-M eluted at a volume 14.5 mL. Protein samples were pooled and stored in the same elution buffer at 4°C. If needed, the protein was concentrated using 100-kDa cutoff centrifugal ultrafiltration concentrator.

4.3 | Evaluation of metal-dependent protein assembly

Of note, 200 μL samples of 20 μM Tet8-M were equilibrated with various concentrations of $NiCl_2$, $CoCl_2$, $CuCl_2$, or $ZnCl_2$ to study the metal-dependent assembly of the protein. Samples were incubated overnight at 4°C with gentle agitation. Samples were analyzed on a superpose-6 10/300 column equilibrated with same Tris–HCl buffer containing the various metal ions at the same concentrations. To study the

stability of assembled protein, the high-molecular-weight complexes eluting at 10.5 mL were re-chromatographed under same buffer conditions.

To further characterize the complexes formed by Tet8-M with Ni^{2+}, the complex was prepared on a larger scale as follows: 400 μL of 50–200 μM protein was incubated with 200 μM $NiCl_2$ overnight at 4°C with gentle agitation and purified by SEC using a superpose-6 10/300 column equilibrated with Tris HCl containing 200 μM $NiCl_2$. The fractions at elution volume 10.5 mL were pooled, concentrated, and used for further characterization by the techniques described below.

4.4 | Cross-linking with BS3 reagent

Assembled cages were cross-linked using the lysine-specific reagent (bis(sulfosuccinimidyl)suberate) (Thermo Fisher) as previously described[22] except that the Tris HCl used for SEC was used for this experiment. These cross-linked cages were visualized by negative-stain TEM and also were used for characterization by (3–12%) native-PAGE.

4.5 | Negative-stain TEM imaging

Negative-stain TEM was performed as previously described.[22] Protein samples were adjusted to a concentration 0.04 mg/mL and fixed on a Formvar/Carbon 400 Mesh Cu grid using conventional negative staining procedures. Imaging was performed using a JEOL 1,500 electron microscope equipped with tungsten filament, XR401 high-sensitivity sCMOS camera and operated at 90 kV.

4.6 | Enzyme activity assays

The esterase activity of the parent TriEst enzyme and the assembled and unassembled Tet8-M were assessed using *2,4*-dinitrophenyl acetate (*2,4*-DNPA) as the substrate and at 45°C as previously described[21] and in Tris HCl SEC buffer. Protein and *2,4*-DNPA concentrations were 1 μM and 1 mM respectively. Activity was monitored by following the increase in absorbance at 405 nm.

4.7 | DLS measurements

DLS was performed using DynaPro NanoStar ZS instrument as previously described.[24] Protein concentrations were adjusted to 20 μM. The samples were centrifuged at $25,000g$ for 10 min to remove any suspended particles. Samples were analyzed in 10 μL cuvettes at 25°C. The refractive index and absorption coefficient for the particles were set at 1.45 and 0.001, respectively. Runs were performed in triplicate, and each run is an average of 10 scans.

ACKNOWLEDGMENTS

CONFLICT OF INTEREST

The authors declare that they have no conflict of interest.

ORCID

E. Neil G. Marsh 🆔 https://orcid.org/0000-0003-1713-1683

REFERENCES

1. Aumiller WM, Uchida M, Douglas T. Protein cage assembly across multiple length scales. Chem Soc Rev. 2018;47:3433–3469.
2. Ma Y, Nolte RJM, Cornelissen JJLM. Virus-based nanocarriers for drug delivery. Adv Drug Deliv Rev. 2012;64:811–825.
3. Schwarz B, Douglas T. Development of virus-like particles for diagnostic and prophylactic biomedical applications: Development of virus-like particles. Wiley Interdiscip Rev Nanomed Nanobiotechnol. 2015;7:722–735.
4. Shirbaghaee Z, Bolhassani A. Different applications of virus-like particles in biology and medicine: Vaccination and delivery systems: Different applications of virus-like particles. Biopolymers. 2016;105:113–132.
5. Lua LHL, Connors NK, Sainsbury F, Chuan YP, Wibowo N, Middelberg APJ. Bioengineering virus-like particles as vaccines: Virus-like particles as vaccines. Biotechnol Bioeng. 2014;111: 425–440.
6. Allen M, Willits D, Mosolf J, Young M, Douglas T. Protein cage constrained synthesis of ferrimagnetic iron oxide nanoparticles. Adv Mater. 2002;14:1562–1565.
7. Bhaskar S, Lim S. Engineering protein nanocages as carriers for biomedical applications. NPG Asia Mater. 2017;9:e371–e371.
8. de la Escosura A, Nolte RJM, Cornelissen JJLM. Viruses and protein cages as nanocontainers and nanoreactors. J Mater Chem. 2009;19:2274.
9. Yildiz I, Shukla S, Steinmetz NF. Applications of viral nanoparticles in medicine. Curr Opin Biotechnol. 2011;22:901–908.
10. Comellas-Aragonès M, de la Escosura A, Dirks A(T)J, et al. Controlled integration of polymers into viral capsids. Biomacromolecules. 2009;10:3141–3147.
11. Kramer RM, Li C, Carter DC, Stone MO, Naik RR. Engineered protein cages for nanomaterial synthesis. J Am Chem Soc. 2004; 126:13282–13286.
12. Uchida M, McCoy K, Fukuto M, et al. Modular self-assembly of protein cage lattices for multistep catalysis. ACS Nano. 2018;12: 942–953.
13. Edwardson TGW, Mori T, Hilvert D. Rational engineering of a designed protein cage for siRNA delivery. J Am Chem Soc. 2018; 140:10439–10442.
14. Bhattacharya P, Du D, Lin Y. Bioinspired nanoscale materials for biomedical and energy applications. J R Soc Interface. 2014;11.
15. Tetter S, Hilvert D. Enzyme encapsulation by a ferritin cage. Angew Chem Int Ed. 2017;56:14933–14936.
16. King NP, Sheffler W, Sawaya MR, et al. Computational design of self-assembling protein nanomaterials with atomic level accuracy. Science. 2012;336:1171–1174.
17. Hsia Y, Bale JB, Gonen S, et al. Design of a hyperstable 60-subunit protein icosahedron. Nature. 2016;535:136–139.
18. Bale JB, Gonen S, Liu Y, et al. Accurate design of megadalton-scale two-component icosahedral protein complexes. Science. 2016;353:389–394.
19. Padilla JE, Colovos C, Yeates TO. Nanohedra: Using symmetry to design self assembling protein cages, layers, crystals, and filaments. Proc Natl Acad Sci U S A. 2001;98:2217–2221.
20. Lai Y-T, Reading E, Hura GL, et al. Structure of a designed protein cage that self-assembles into a highly porous cube. Nat Chem. 2014;6:1065–1071.
21. Sciore A, Su M, Koldewey P, et al. Flexible, symmetry-directed approach to assembling protein cages. Proc Natl Acad Sci U S A. 2016;113:8681–8686.
22. Badieyan S, Sciore A, Eschweiler JD, et al. Symmetry-directed self-assembly of a tetrahedral protein cage mediated by de novo-designed coiled coils. Chembiochem. 2017;18:1888–1892.
23. Cristie-David AS, Chen J, Nowak DB, et al. Coiled-coil-mediated assembly of an icosahedral protein cage with extremely high thermal and chemical stability. J Am Chem Soc. 2019;141: 9207–9216.
24. Cristie-David AS, Koldewey P, Meinen BA, Bardwell JCA, Marsh ENG. Elaborating a coiled coil-assembled octahedral protein cage with additional protein domains: A multi-domain coiled coil-assembled protein cage. Protein Sci. 2018;27:1883–1890.
25. Patterson DP, Su M, Franzmann TM, Sciore A, Skiniotis G, Marsh ENG. Characterization of a highly flexible self-assembling protein system designed to form nanocages: Highly flexible self-assembling protein system. Protein Sci. 2014;23:190–199.
26. Patterson DP, Desai AM, Holl MMB, Marsh ENG. Evaluation of a symmetry-based strategy for assembling protein complexes. RSC Adv. 2011;1:1004–1012.
27. Dominguez R, Holmes KC. Actin structure and function. Annu Rev Biophys. 2011;40:169–186.
28. Otsuka S, Ellenberg J. Mechanisms of nuclear pore complex assembly—Two different ways of building one molecular machine. FEBS Lett. 2018;592:475–488.
29. Shoemaker GK, van Duijn E, Crawford SE, et al. Norwalk virus assembly and stability monitored by mass spectrometry. Mol Cell Proteomics. 2010;9:1742–1751.
30. Zhang W, Luo Q, Miao L, et al. Self-assembly of glutathione S-transferase into nanowires. Nanoscale. 2012;4:5847–5851.
31. Scotter AJ, Guo M, Tomczak MM, et al. Metal ion-dependent, reversible, protein filament formation by a designed beta-roll polypeptide. BMC Struct Biol. 2007;7:63.
32. Ringler P, Schulz G. Self-assembly of proteins into designed networks. Science. 2003;302:106–109.
33. Suzuki Y, Cardone G, Restrepo D, Zavattieri PD, Baker TS, Tezcan FA. Self-assembly of coherently dynamic, auxetic, two-dimensional protein crystals. Nature. 2016;533:369–373.
34. Bailey JB, Zhang L, Chiong JA, Ahn S, Tezcan FA. Synthetic modularity of protein–metal–organic frameworks. J Am Chem Soc. 2017;139:8160–8166.

35. Liljeström V, Mikkilä J, Kostiainen MA. Self-assembly and modular functionalization of three-dimensional crystals from oppositely charged proteins. Nat Commun. 2014;5:445.

36. Sontz PA, Bailey JB, Ahn S, Tezcan FA. A metal organic framework with spherical protein nodes: Rational chemical design of 3D protein crystals. J Am Chem Soc. 2015;137:11598–11601.

37. Ballister ER, Lai AH, Zuckermann RN, Cheng Y, Mougous JD. In vitro self-assembly of tailorable nanotubes from a simple protein building block. Proc Natl Acad Sci U S A. 2008;105: 3733–3738.

38. Moll D, Huber C, Schlegel B, Pum D, Sleytr UB, Sára M. S-layer-streptavidin fusion proteins as template for nanopatterned molecular arrays. Proc Natl Acad Sci U S A. 2002;99: 14646–14651.

39. Schurke P, Freeman JC, Dabrowski MJ, Atkins WM. Metal-dependent self-assembly of protein tubes from *Escherichia coli* glutamine synthetase: Cu^{2+} EPR studies of the ligation and stoichiometry of intermolecular metal binding sites. J Biol Chem. 1999;274:27963–27968.

40. Bailey JB, Subramanian RH, Churchfield LA, Tezcan FA. FA metal-directed design of supramolecular protein assemblies. Methods Enzymol. 2016;580:223–250.

41. Huard DJE, Kane KM, Tezcan FA. Re-engineering protein interfaces yields copper-inducible ferritin cage assembly. Nat Chem Biol. 2013;9:169–176.

42. Choi S-H, Choi K, Chan Kwon I, Ahn HJ. The incorporation of GALA peptide into a protein cage for an acid-inducible molecular switch. Biomaterials. 2010;31:5191–5198.

43. Malay AD, Miyazaki N, Biela A, et al. An ultra-stable gold-coordinated protein cage displaying reversible assembly. Nature. 2019;569:438–442.

44. Suzuki K, Hiroaki H, Kohda D, Nakamura H, Tanaka T. Metal ion induced self-assembly of a designed peptide into a triple-stranded α-helical bundle: A novel metal binding site in the hydrophobic core. J Am Chem Soc. 1998;120:13008–13015.

45. Ozaki E, Sakimae A. Purification and characterization of recombinant esterase from Pseudomonas putida MR-2068 and its application to the optical resolution of dimethyl methylsuccinate. J Biosci Bioeng. 1997;83:535–539.

46. Shaw S-Y, Chen Y-J, Ou J-J, Ho L. Enzymatic resolution of methyl dl-β-acetylthioisobutyrate and dl-β-acetylthioisobutyramide using a stereoselective esterase from Pseudomonas putida IFO12996. J Mol Catal B Enzym. 2006;38:163–170.

SUPPORTING INFORMATION

Additional supporting information may be found online in the Supporting Information section at the end of this article.